VALENCE BAND OFFSET AND HOLE TRANSPORT ACROSS a-SiO$_x$ (0<x<2) PASSIVATION LAYERS IN SILICON HETEROJUNCTION SOLAR CELLS

Martin Liebhaber[*,1], Mathias Mews[2], Lars Korte[2], Tim F. Schulze[1], Bernd Rech[2], and Klaus Lips[1]

[1] Institute for Nanospectroscopy, Helmholtz-Zentrum Berlin, Albert-Einstein-Straße 15, D-12489 Berlin, Germany
[2] Institute for Silicon Photovoltaics, Helmholtz-Zentrum Berlin, Kekuléstraße 5, D-12489 Berlin, Germany
[*] Corresponding author e-mail: martin.liebhaber@helmholtz-berlin.de

ABSTRACT: In this work, the valence band offset (ΔE_V) and hole transport across the heterojunction between amorphous silicon suboxides (a-SiO$_x$:H) and crystalline silicon (c-Si) is investigated. Thin layers ranging from pure intrinsic a-Si:H to near-stoichiometric a-SiO$_2$ were grown by varying precursor gas mixtures during chemical vapor deposition. A continuous increase of ΔE_V starting from ≈ 0.3 eV for the a-Si:H/c-Si to > 4 eV for the a-SiO$_2$/c-Si heterointerface was measured by *in-system* photoelectron spectroscopy. Furthermore, (p)a-Si:H/(i)a-SiO$_x$:H/(n)c-Si/(i,n$^+$)a-Si:H heterojunction solar cells, with intrinsic a-SiO$_x$:H passivation layers deposited using the same parameter sets, were fabricated. We report a linear decrease of the solar cell fill factor for increasing ΔE_V in the range of 0.27 – 0.85 eV. The reason is an increase of the barrier height for holes at the (i)a-SiO$_x$:H/(n)c-Si heterojunction and a simultaneous change of the hole transport mechanism from thermionic emission to defect-assisted tunnel hopping through valence-band tail-states. It is demonstrated that as compared to a single layer, significantly larger barrier heights can be tolerated in a stack of high band gap material and a material with lower band gap, forming a staircase of band offsets. This could allow the application of these layers in silicon heterojunction solar cells.
Keywords: amorphous/crystalline silicon heterojunctions, silicon solar cells, valence band offset, carrier transport

1 INTRODUCTION

Although a large variety of alternative material systems and photovoltaic (PV) technologies were rising up in the past [1] it seems that on an industrial, low cost and large scale level, silicon wafer based PV approaches cannot be beaten in the near future [2]. Among those, the amorphous/crystalline silicon heterojunction (SHJ) solar cell is a promising approach, which is reflected in the actual efficiency record of 24.7 % for a standard cell design with a p/n junction on the front and a back surface field on the rear side of the cell, respectively [3]. This structure is depicted in Fig. 1(a), which is the layer stack used in our study. For an interdigitated back contact design the world record efficiency of 25.6 % for a PV device with a single p/n junction was reported in 2014 by Panasonic [4]. These high efficiencies, which are already close to the theoretical Shockley-Queisser limit of 29 % for single-junction silicon solar cells [5] can be achieved mainly due to the excellent and full area passivated contacts. However, a drawback of this technology is the current loss due to parasitic absorption in the amorphous silicon emitter and passivation layers on the front side of the standard cell design (cf. Fig. 1(a)). Holman *et al.* calculated total current density losses of about 1.2 mA/cm^2 in 5 nm (p)a-Si:H and about 0.6 mA/cm^2 in 5 nm (i)a-Si:H [6]. Therefore, one possibility to further improve this technology could be the replacement of these a-Si:H layers by higher band gap and low absorption a-Si:H alloys like amorphous or microcrystalline silicon oxide (a-SiO$_x$:H) [7-10] or silicon carbide [11, 12].

In this paper we reconsider the results of our fundamental study of (i)a-SiO$_x$ layers deposited on (n)c-Si wafers [13]. The stoichiometry *x* of these passivation layers, as well as the valence band (VB) offset ΔE_V at the SHJ (cf. Fig. 1(b)) was determined. In a second step, SHJ solar cells with identically prepared passivation layers were fabricated [14]. We can directly link ΔE_V at the SHJ to solar cell performance, since ΔE_V constitutes a transport barrier for holes, which is reflected in the solar cell's fill factor. In Fig. 1(b) the band line-up of the SHJ is sketched. Hole transport from the c-Si absorber to the front contact can occur either by thermionic emission or by defect-assisted tunnel hopping processes through the (i)a-SiO$_x$ passivation layer, depending on the transport barrier height imposed by ΔE_V [15-17].

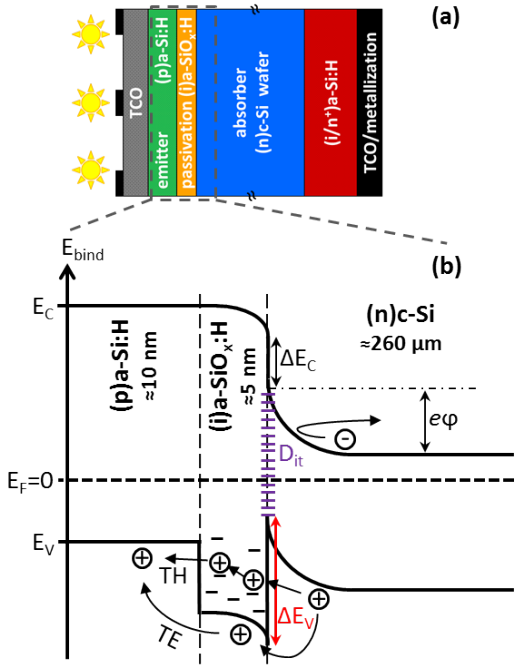

Figure 1: (a) Basic structure of the investigated a-Si:H/c-Si heterojunction (SHJ) solar cell (layer thicknesses not to scale). (b) Band line-up at the hole contact of the SHJ solar cell. Holes which are generated in the (n)c-Si absorber can overcome the transport barrier imposed by the valence band offset ΔE_V either by thermionic emission (TE) across, or by tunnel-hopping processes (TH) through the (i)a-SiO$_x$:H passivation layer. They then travel in the (p)a-Si:H valence band and are collected at the external front contact (TCO and metal grid). The sketch also shows other relevant physical quantities like the band bending $e\varphi$ and interface defect density D_{it}.

The aim of this report is to summarize our results of the evolution of ΔE_V and the passivation properties at the (i)a-SiO_x/(n)c-Si heterointerface with changing stoichiometry *x* [13], and the direct correlation of these SHJ parameters to solar cell performance [14]. This direct correlation of junction parameters with device results is a significant added value in comparison to former studies [7-9]. We are thus able to discuss the hole transport mechanisms across the SHJ, which is still a subject of discussion, in more detail. Finally we will comment on possibilities for implementation of high band gap materials in SHJ devices.

2 EXPERIMENTAL

2.1 Layer deposition and solar cell fabrication

The substrates used in our study were commercial available high quality float zone silicon wafers, 260 µm thick, polished with a (111) surface orientation and a resistivity of ≈ 3 Ω·cm (phosphorus-doped). With the standard RCA process, the wafers were cleaned, followed by a dip in diluted hydrofluoric acid (1%, 2 min) to remove the native silicon oxide.

Amorphous layers were grown with conventional parallel plate (2 cm electrode distance) plasma-enhanced chemical vapour deposition (PECVD) at 60 MHz excitation, a plasma power density of 56 mW/cm^2, a process pressure of 0.5 mbar, a substrate temperature of 175 °C, and precursor gas mixtures of $SiH_4/CO_2/H_2$. For hydrogen passivation the gas flow of H_2 was kept constant at 5 sccm. SiH_4 and CO_2 gas flows added up to a total of 10 sccm. In order to vary the stoichiometry *x* of our (i)a-SiO_x:H layers, the ratio $R = CO_2/SiH_4$ was varied from 0 to 4, as it is also depicted by the bars in Fig. 3. Layer thicknesses were determined by using spectroscopic ellipsometry (wavelength range 190 – 850 nm) and fitting the data with a Tauc-Lorentz model [18].

For solar cell fabrication, as its structure is depicted in Fig. 1(a), on the rear side wafers were coated with 4 nm intrinsic a-Si:H and a 8 nm n^+-type a-Si:H layer to act as a back surface field. On the front side, 5 nm intrinsic a-SiO_x:H passivation and 8 nm p-type a-Si:H emitter layers were deposited. The solar cells were then completed by ITO sputtering and metallization with Ti/Ag stacks as it is described elsewhere [19]. Note that for photoelectron spectroscopy (PES) analysis thicker layers of 10 nm (i)a-SiO_x (due to information depth of analysing methods) were grown using the same parameter sets.

2.2 Analysing methods

Layer properties during cell fabrication, as well as heterojunction parameters were analysed with various methods.

Photoconductance decay (PCD) measurements from which we can extract minority carrier lifetimes and interface defect densities D_{it}, and illumination dependent open circuit voltage measurements ($SunsV_{OC}$) [20] were carried out in between various process steps. To quantify the surface band bending $e\varphi$ of c-Si in equilibrium, the surface photovoltage (SPV) method [21] was employed.

Different modes of *in-system* PES were conducted to determine the VB edge position, as well as the stoichiometry *x* of the (i)a-SiO_x:H layers. In order to avoid surface oxidation and other contamination by surface adsorbates, a vacuum transfer of the samples from the PECVD to the ultrahigh vacuum analysis chamber was achieved. The stoichiometry was quantified by using Mg K_α X-ray PES (XPS). Near-ultraviolet PES measurements using a high pressure Xe-lamp and a double grating monochromator (4.0 – 7.3 eV excitation energy) were conducted in the constant-final-state-yield mode (CFSYS) [22] to resolve the valence band region. The VB tail (Urbach Energy E_{0V}) and edge position was determined by fitting a model density of states (DOS) to the data [23]. For layers with VB offsets larger than 1.24 eV, the low excitation energy of this method was not sufficient enough to further track the VB edge. Therefore, we employed the less sensitive ultraviolet PES (UPS) method, using a He-lamp (He-I discharge line at 21.2 eV).

For discussion of our experimental data, numerical device simulations were carried out using the software AFORS-HET [24].

3 RESULTS AND DISCUSSION

3.1 a-SiO_x:H film and SHJ characterization

In the first part of this report, the (i)a-SiO_x films itself (stoichiometry *x* and VB structure) and relevant a-SiO_x/c-Si heterojunction parameters (VB offset ΔE_V and passivation quality D_{it}) are characterized. For a comprehensive discussion of this part see Ref. [13].

Based on an XPS analysis, we monitor in a first step the evolution of the stoichiometry *x* of our (i)a-SiO_x:H layers. Fig. 2(a) shows the raw data of the Si 2p peak. For pure (i)a-Si:H (0 sccm CO_2, black curve in Fig. 2(a)) there is only one peak (Si^{0+}) in the spectra located at approx. 99.4 eV (spin-orbit splitted into Si $2p_{3/2}$ and Si $2p_{1/2}$, cf. Fig. 2(b)). For increasing CO_2 flow the chemical environment of the Si atoms changes and therefore the Si^{0+} peak is gradually reduced and coincidently peaks corresponding to core level signals from the various Si oxidation states (Si^{1+}… Si^{4+}) appear on the higher binding energy side between 101 – 104 eV. An exemplarily curve is shown in Fig. 2(b) with fixed Si suboxide peak positions fitted using tabulated values [25]. Following this well-established fitting analysis, the stoichiometry *x* of the films can be calculated based on the ratio of various suboxide peak areas by using the formula [25]:

$$\frac{O}{Si} = \frac{1}{2}\sum_{j=0}^{4} j \cdot \frac{A_j}{A_{total}}$$

where *j* denotes the various oxidation states with their corresponding peak areas A_j. This procedure is cross-checked with a complementary method based on the O 1s/Si 2s peak ratios weighted with their respective atomic sensitivity factors [26]. Fig. 3 shows the resulting calibration curve, in which the precursor gas flows of SiH_4 and CO_2 respectively in the PECVD can be directly linked to the corresponding film stoichiometry *x*. Our layers range from pure a-Si:H to nearly stoichiometric a-SiO_2. Note that for all layers the C concentration stayed well below 3 % of the O concentration.

In a next step we investigated the changes in the VB structure of the (i)a-SiO_x:H layers over the whole stoichiometry range ($0 \leq x \lesssim 2$) by using various modes of ultraviolet PES. Fig. 4(a) shows the raw data of the near-ultraviolet PES in the so-called CFSYS mode [22]. The inset displays a typical a-Si:H DOS spectrum and a model DOS obtained by a fit procedure as has been

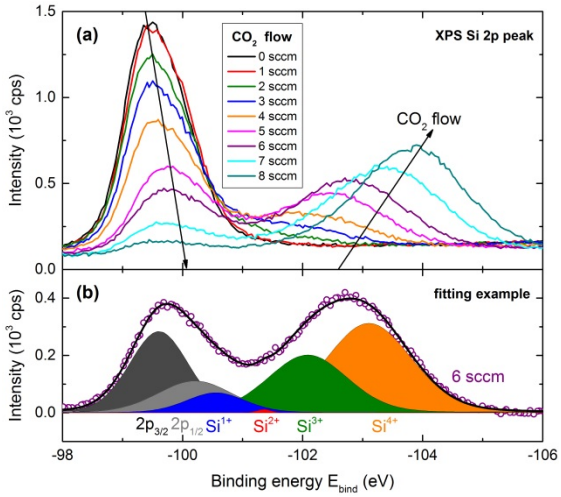

Figure 2: (a) XPS raw data of the Si 2p peak for (i)a-SiO_x:H layers deposited with different precursor gas flow rates of SiH_4/CO_2. (b) Exemplary peak fit for 6 sccm CO_2 flow showing the different Si oxidation states. Composition and peak shift result from changes in the chemical near-field surrounding of Si upon O incorporation.

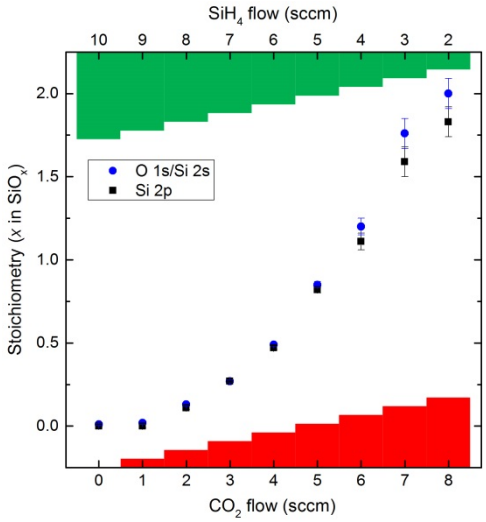

Figure 3: Stoichiometry *x* of (i)a-SiO_x:H films in dependence of the SiH_4/CO_2 precursor gas flow ratios (green and red bars) during layer deposition as deduced from XPS data analysis using either the ratios of the O 1s to the Si 2s peak areas (blue points) or the relative contributions of the Si oxidation states in the Si 2p peak (black squares).

discussed and evaluated earlier [23]. By modeling the CFSYS data the VB edge positions (points in Fig. 4 (a)), its exponentially decaying tail slopes (Urbach energies) and the mid-gap dangling bond defect distributions can be obtained (cf. Ref. [13]). With increasing O concentration the VB edge position steadily increases, and eventually for values $x > 0.84$ it is shifted too far towards higher binding energies and thus beyond the range accessible with the UV lamp used in this study (excitation energies between 4.0 – 7.3 eV). Therefore, to further track the evolution of the VB edge position, the standard He-UPS method with a higher excitation energy of 21.2 eV was conducted. The VB edge position is determined by a linear extrapolation of the DOS leading edge to zero, but due to the lack of signal-to-noise VB tails or dangling bonds cannot be resolved for these measurements (Fig. 4(b)). Moreover, at the a-$SiO_{0.84}$:H sample we applied both methods and found an agreement within 0.3 eV, which we also take as an estimate for the systematic error of our PES study.

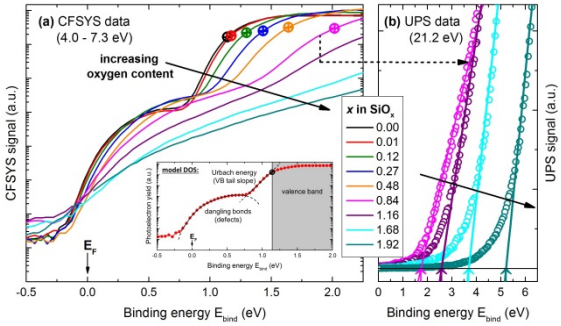

Figure 4: (a) CFSYS spectra of the VB DOS for the a-SiO_x:H layers with different stoichiometry *x*. The inset shows a model fit of a typical a-Si:H DOS consisting of a broad dangling bond defect distribution and the exponential decaying VB tail (Urbach energy) [23]. The VB edge positions are denoted by the dots. A continuous shift to higher binding energies for increasing O contents is observed. (b) UPS data in which the VB edge positions (arrow marks) are obtained by linear extrapolation of the leading edge to zero.

In order to determine the relevant heterojunction parameter ΔE_V, we need to further consider possible changes of the *equilibrium band bending* $e\varphi$ (cf. Fig. 1(b)). Therefore SPV measurements, performed on the PES samples immediately after removal from the UHV system, were conducted. For all samples $e\varphi$ stayed below 0.15 eV and the values are taken into account by using the formula (cf. Fig. 1(b)):

$$\Delta E_V = E_{V,a-SiO_x:H} - E_{V,c-Si} + e\varphi$$

Fig. 5(a) displays the resulting VB offsets ΔE_V, calculated by combining PES and SPV results, and plotted against the stoichiometry *x*, determined by XPS measurements. Our values start at the standard value of $\Delta E_V \approx 0.3$ eV for pure a-Si and monotonously rises for increasing stoichiometry *x* to more than 4.0 eV for the near-stoichiometric a-SiO_2 layers. Concerning these end points, our results are in line with literature data [21, 23, 27, 28].

Finally, we turn to the analysis of the (i)a-SiO_x interface passivation of the c-Si substrate, as sufficient good passivation qualities are crucial for a successful device implementation of these layers. Fig. 5(b) displays the interface defect density D_{it}, as it is extracted from the injection dependence of the minority carrier lifetime measured with PCD on solar cell precursors with an (i)a-Si:H passivation and a (n^+)a-Si:H layer stack on the back side, and an (i)a-SiO_x:H layer on the front side. As depicted in Fig. 5, data are only shown for the device relevant low-*x* regime. It is obvious that D_{it} increases drastically for rising O concentration, but also decreases to the same order of magnitude after (p)a-Si:H emitter deposition on top of the (i)a-SiO_x passivation layers. After emitter deposition all (i)a-SiO_x layers show a similar passivation quality as the standard (i)a-Si:H/c-Si interface (without O) which is promising with respect to device application. Note that the samples in this study are not symmetric which may lead to a slightly overestimation of 10 % for the calculated D_{it} [14]. D_{it} can be directly related to the Si bonding environment and the H density at the SHJ. During (p)a-Si:H deposition, the sample temperature stays below 200 °C, i.e. below the temperature that is required for thermal activation of bond reconfiguration in an annealing step. Thus, it can be

surmised that the lowered dangling bond concentration at the interface, as evidenced by the reduced D_{it}, is likely due to dangling bond saturation with H provided during the additional plasma process [14].

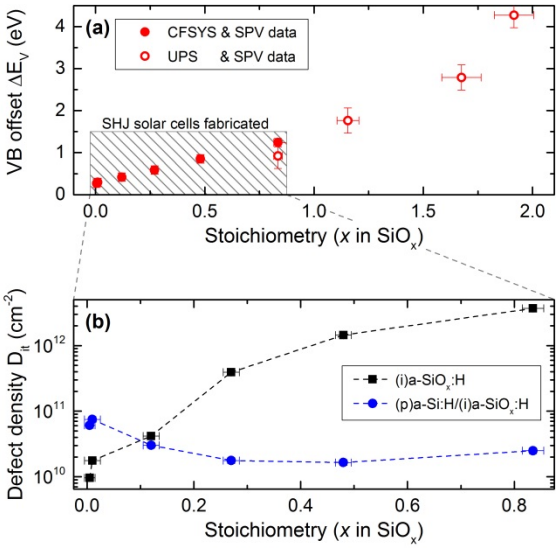

Figure 5: (a) VB offset ΔE_V at the a-SiO_x:H/c-Si heterojunction derived from combining PES and SPV data for the whole stoichiometry range ($0 \leq x \lesssim 2$). (b) Interface defect density D_{it} obtained from PCD measurements for c-Si passivated with (i)a-SiO_x:H (black squares) and after subsequent (p)a-Si:H emitter deposition on the same samples (blue circles). Data shown in (b) only for the low-*x* stoichiometry range ($x \leq 0.84$) which is relevant for SHJ solar cells.

3.2 a-SiO_x:H passivation layers in SHJ solar cells

In the second part of this report we discuss the implementation of identically prepared (i)a-SiO_x:H layers (low-*x* regime) as passivation layers in SHJ solar cells. Therefore we are able to directly connect the measured ΔE_V to device performance. A more detailed discussion of this part can be found in Ref. [14]

Fig. 6(a) displays the experimental I-V-characteristics of SHJ solar cells measured at AM1.5 irradiation. The most prominent feature is the strongly increasing s-shape of the I-V-curves for rising ΔE_V. Fig. 6(b) shows the solar cell's V_{OC} and implied V_{OC} (iV_{OC}), measured at cell precursors before ITO deposition and metallization. V_{OC} decrease slightly and monotonously for rising ΔE_V, whereas the iV_{OC} stays constant after an initial increase. This behavior is explained with an increased layer porosity for films with higher oxygen fractions. Depending on the morphology, hydrogen is driven out in the following processes, causing slightly poorer passivation quality and resulting in the observed decrease in V_{OC} (cf. Ref [14] & references therein). In Fig. 6(c) the FF and pseudo FF (pFF) of the solar cells, as well as simulated FF (sFF) are plotted against ΔE_V. At first sight the pronounced difference between the strongly decreasing FF and the even slightly increasing pFF might be unexpected. The pFF is measured using $SunsV_{OC}$, where no current is extracted from the device. It reflects the maximum possible FF, excluding carrier transport related effects. Therefore, we relate the strongly decreasing FF from 78 % at ΔE_V = 0.27 eV to 52 % for ΔE_V = 1.24 eV to a transport barrier for charge extraction through the heterointerface, due to the increasing VB offset ΔE_V at the SHJ. Numerical simulations were conducted to gain further insight into the dependence of the hole transport mechanism on ΔE_V. Using the software AFORS-HET [24] only thermionic emission is employed to simulate the transport across the SHJ, which is a commonly used assumption in literature [9, 29]. It is obvious from Fig. 6(c), that this assumption only fits the experimental data for ΔE_V values well below 400 meV. Therefore, in this regime thermionic emission appears to be the dominant transport mechanism. For higher VB offsets additional pathways for the minority charge carrier transport must exist. These are commonly assumed to be defect-assisted tunnel hopping processes through the VB tail states of the amorphous passivation layers. From the comparison between the experimental findings presented here and simulation studies [14-17, 30] we conclude that for $\Delta E_V \gtrsim 400$ meV tunneling processes at the interface become dominant. However, this additional transport path is not conductive enough to prevent a degradation of the FF, which results in reduced solar cell performance.

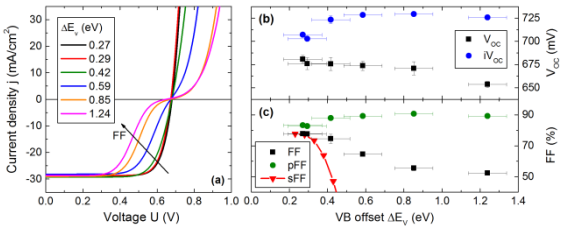

Figure 6: (a) I-V-characteristics under AM1.5 spectrum irradiation of SHJ solar cells with differen (i)a-SiO_x passivation layers and thus varying VB offsets ΔE_V. (b) Open circuit voltage (V_{OC}) and implied V_{OC} (iV_{OC}). (c) Solar cell fill factor (FF) and $SunsV_{OC}$ pseudo FF (pFF) for the same solar cells, and simulated FF (sFF) using AFORS-HET.

This transport problem across the SHJ for larger VB offsets hampers the application of wide band gap materials (such as a-SiO_x) in solar cell devices. To mitigate this problem, we pursued the idea to split the total VB offset at the c-Si/wide-gap material interface into a sequence of two smaller offsets. To this end, as a proof of concept, we fabricated SHJ solar cells with a layer stack on the front side consisting of a 2 nm (i)a-Si:H passivation layer with a VB offset to the c-Si substrate of ΔE_V = (270 ± 50) meV, followed by a 3 nm thick (i)a-$SiO_{0.3}$:H layer. For this structure (inset of Fig. 7) we determined a total VB offset of ΔE_V = (585 ± 50) meV. The resulting I-V-curve of this a-Si:H/a-$SiO_{0.3}$:H *staircase approach* is compared to the single layer a-$SiO_{0.3}$:H reference cell in Fig. 7(a). It is obvious that the relatively low FF of 63 %, caused by the transport barrier at the heterojunction of ΔE_V = (585 ± 50) meV, can be drastically increased by splitting this VB offset. Apparently, in the stacked device the transport barrier is reduced and therefore the FF increases significantly to 70 %. Note that this increased FF is still on a somewhat lower level as our standard cell with 5 nm (i)a-Si:H passivation layer yielding a FF of 78 %. The V_{OC} of the two cells are identical, indicating comparable passivation qualities. Nevertheless, these results reveal that the stacked layer approach is a promising concept with respect to device application. In addition, we also conducted numerical simulations with AFORS-HET. As for the single layers in the previous section, only thermionic emission as transport mechanism over the SHJ was implemented in our simulations. For the stack, the total VB offset is plotted on the abscissa, which is split into the fixed 270 meV offset of the a-Si:H/c-Si interface and a second offset, summing up to the total ΔE_V. The obtained

FF values are depicted in Fig. 7(b). As expected, a material stack approach does not change the overall trend of decreasing FF for increasing ΔE_V, but increases the FF at a given overall VB offset. Since our simulations do not include any hopping processes, this constitutes a clear indication that the increasing FF is most likely due to more efficient thermionic emission along a layer stack, than for a single interface with only one large VB offset. Note that at this point we do not consider any tunnel-hopping effects in the 3 nm reduced oxide layer thickness compared to the standardly used 5 nm thicknesses in the single layer approach (cf. Ref. [14]).

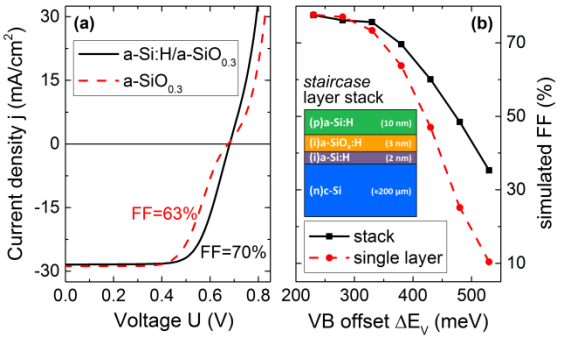

Figure 7: (a) I-V-characteristics under AM1.5 spectrum irradiation of SHJ solar cells with a single 5 nm thick (i)a-$SiO_{0.3}$:H passivation layer (dashed red curve) corresponding to a VB offset ΔE_V = (585 ± 50) meV and a *staircase* passivation layer stack (black curve) with the same overall ΔE_V but split into 2 nm (i)a-Si:H with ΔE_V = (270 ± 50) meV and 3 nm of (i)a-$SiO_{0.3}$:H. (b) Simulated FFs extracted from AFORS-HET simulations implementing only thermionic emission over the (i)a-SiO_x:H/c-Si interface for variable ΔE_V (dashed red curve) and the same simulations for the (i)a-$SiO_{0.3}$:H/(i)a-Si:H/c-Si layer stack where the total ΔE_V is plotted on the abscissa.

3 CONCLUSION

One possibility to further improve the high efficient silicon heterojunction (SHJ) solar cell concept is to reduce the parasitic absorption in its front contact layers by implementing wider band gap materials which will obviously also modify the band alignment at the heterointerface. In our studies we investigated a-SiO_x:H, ranging from pure a-Si to wide band gap near-stoichiometric a-SiO_2. Layers were prepared with plasma enhanced chemical vapour deposition by varying the precursor gas fraction of SiH_4/CO_2. Film stoichiometry and valence band alignment at the SHJ was investigated via various modes of *in-system* photoelectron spectroscopy. Furthermore, all our layers reveal a sufficient surface passivation. In a second step SHJ solar cells with identically prepared layers were fabricated. Therefore, we can directly relate the measured valence band offsets at the heterointerface to solar cell parameters. Rising valence band offsets cause increasing transport barriers for holes. This is reflected in decreasing solar cell fill factors. The experimental results are compared and discussed with the aid of numerical simulations. Device efficiencies decrease for increasing transport barriers due to a decreasing contribution of thermionic emission. Simultaneously the contribution of tunneling processes increases. This constitutes a general problem for SHJ solar cells. Nevertheless, we demonstrate that a stacked passivation layer approach mitigates this transport problem. Layer stacking and therefore the splitting of valence band offsets is a promising concept. Especially, the combination of a medium band gap passivation layer and a high band gap hole contact layer could allow the successful application in SHJ devices.

ACKNOWLEDGEMENTS

The authors would like to thank Thomas Lußky, Erhard Conrad, Kerstin Jacob, and Mona Wittig for technical assistance. This study was partly financed by the German Federal Ministry for Research and Education through the project SISSY (Grant No. BMBF-03SF0403) and the European Commission through the FP7-ENERGY Project HERCULES (Grant No. 608498).

REFERENCES

[1] *Best Research-Cell Efficiencies (NREL.gov)* (2015).
[2] *International Technology Roadmap for Photovoltaic, Sixth Edition (ITRPV.net)* (2015).
[3] Taguchi, M., Yano, A., Tohoda, S., Matsuyama, K., Nakamura, Y., Nishiwaki, T., Fujita, K., and Maruyama, E. *IEEE J. Photovoltaics* **4**, 96–99 (2014).
[4] Masuko, K., Shigematsu, M., Hashiguchi, T., Fujishima, D., Kai, M., Yoshimura, N., Yamaguchi, T., Ichihashi, Y., Mishima, T., Matsubara, N., Yamanishi, T., Takahama, T., Taguchi, M., Maruyama, E., and Okamoto, S. *IEEE J. Photovoltaics* **4**, 1433 (2014).
[5] Shockley, W. and Queisser, H. J. *J. Appl. Phys.* **32**, 510 (1961).
[6] Holman, Z. C., Descoeudres, A., Barraud, L., Fernandez, F. Z., Seif, J. P., De Wolf, S., and Ballif, C. *IEEE J. Photovoltaics* **2**, 7 (2012).
[7] Fujiwara, H., Kaneko, T., and Kondo, M. *Appl. Phys. Lett.* **91**, 133508 (2007).
[8] Ding, K., Aeberhard, U., Finger, F., and Rau, U. *J. Appl. Phys.* **113**, 134501 (2013).
[9] Seif, J. P., Descoeudres, A., Filipic, M., Smole, F., Topic, M., Holman, Z. C., De Wolf, S., and Ballif, C. *J. Appl. Phys.* **115**, 024502 (2014).
[10] Mazzarella, L., Kirner, S., Stannowski, B., Korte, L., Rech, B., and Schlatmann, R. *Appl. Phys. Lett.* **106**, 023902 (2015).
[11] Zhang, D., Deligiannis, D., Papakonstantinou, G., van Swaaij, R. A. C. M. M., and Zeman, M. *IEEE J. Photovoltaics* **4**, 1326 (2014).
[12] Boccard, M. and Holman, Z. C. *J. Appl. Phys.* **118**, 065704 (2015).
[13] Liebhaber, M., Mews, M., Schulze, T. F., Korte, L., Rech, B., and Lips, K. *Appl. Phys. Lett.* **106**, 031601 (2015).
[14] Mews, M., Liebhaber, M., Rech, B., and Korte, L. *Appl. Phys. Lett.* **107**, 013902 (2015).
[15] Kanevce, A. and Metzger, W. K. *J. Appl. Phys.* **105**, 094507 (2009).
[16] Rahmouni, M., Datta, A., Chatterjee, P., Damon-Lacoste, J., Ballif, C., and i Cabarrocas, P. R. *J. Appl. Phys.* **107**, 054521 (2010).
[17] van Cleef, M. W. M., Schropp, R. E. I., and Rubinelli, F. A. *Applied Physics Letters* **73**, 2609 (1998).
[18] Jellison, G. E. and Modine, F. A. *Appl. Phys. Lett.* **69**, 371 (1996).
[19] Mews, M., Leendertz, C., Algasinger, M., Koynov, S., and Korte, L. *Phys. Status Solidi (RRL)* **8**, 831 (2014).

[20] Sinton, R. A. and Cuevas, A. *Appl. Phys. Lett.* **69**, 2510 (1996).
[21] Schulze, T. F., Korte, L., Ruske, F., and Rech, B. *Phys. Rev. B* **83**, 165314 (2011).
[22] Sebastiani, M., Gaspare, L. D., Capellini, G., Bittencourt, C., and Evangelisti, F. *Phys. Rev. Lett.* **75**, 3352 (1995).
[23] Korte, L. and Schmidt, M. *J. Appl. Phys.* **109**, 063714 (2011).
[24] Varache, R., Leendertz, C., Gueunier-Farret, M., Haschke, J., Muñoz, D., and Korte, L. *Sol. Energy Mater. Sol. Cells* **141**, 14 (2015).
[25] Himpsel, F. J., McFeely, F. R., Taleb-Ibrahimi, A., Yarmoff, J. A., and Hollinger, G. *Phys. Rev. B* **38**, 6084 Sep (1988).
[26] Wagner, C., Davis, L., Zeller, M., Taylor, J., Raymond, R., and Gale, L. *Surf. Interface Anal.* **3**, 211 (1981).
[27] Nohira, H., Omura, A., Katayama, M., and Hattori, T. *Appl. Surf. Sci.* **123**, 546–549 (1998).
[28] Keister, J., Rowe, J., Kolodziej, J., Niimi, H., Madey, T., and Lucovsky, G. *J. Vac. Sci. Technol. B* **17**(4), 1831–1835 (1999).
[29] Datta, A., Rahmouni, M., Nath, M., Boubekri, R., i Cabarrocas, P. R., and Chatterjee, P. *Sol. Energy Mater. Sol. Cells* **94**, 1457 (2010).
[30] Crandall, R. S., Iwaniczko, E., Li, J. V., and Page, M. R. *J. Appl. Phys.* **112**, 093713 (2012).